

Obtaining Subwavelength Optical Spots Using Nanoscale Ridge Apertures

E. X. Jin

e-mail: xjin@purdue.edu

X. Xu¹

e-mail: xxu@ecn.purdue.edu

School of Mechanical Engineering,
Purdue University,
West Lafayette, IN 47907

Concentrating light into a nanometer domain is needed for optically based materials processing at the nanoscale. Conventional nanometer-sized apertures suffer from low light transmission, therefore poor near-field radiation. It has been suggested that ridge apertures in various shapes can provide enhanced transmission while maintaining the subwavelength optical resolution. In this work, the near-field radiation from an H-shaped ridge nanoaperture fabricated in an aluminum thin film is experimentally characterized using near-field scanning optical microscopy. With the incident light polarized along the direction across the gap in the H aperture, the H aperture is capable of providing an optical spot of about 106 nm by 80 nm in full-width half-maximum size, which is comparable to its gap size and substantially smaller than those obtained from the square and rectangular apertures of the same opening area. Finite different time domain simulations are used to explain the experimental results. Variations between the spot sizes obtained from a 3 × 3 array of H apertures are about 4–6%. The consistency and reliability of the near-field radiation from the H apertures show their potential as an efficient near-field light source for materials processing at the nanoscale. [DOI: 10.1115/1.2401196]

1 Introduction

There has been a continuous need to increase the areal density of microelectronic devices. To further increase the areal density without relying on expensive light sources of shorter wavelength, one has to seek nonconventional approaches, for examples, solid immersion lens [1], and optical near-field techniques [2,3]. In the near-field optical approach, a subwavelength aperture in an opaque metal film is often used as a radiation transducer. It converts far-field radiation to spatially confined near-field radiation, and provides a subdiffraction-limited light source whose resolution depends on the size of the aperture instead of the wavelength of light. The re-radiated field from the subwavelength aperture is localized in the vicinity of the aperture, so the material to be processed is brought close to the metal film at a distance less than the wavelength of light. For example, a very small aperture laser (VSAL) has been proposed to achieve optical storage density exceeding tens of Gb/in.² [4]. To reach higher areal density, the physical size of the aperture has to be reduced to much less than the diffraction limit. However, according to the standard aperture theory [5], the light transmission through a small hole decays as a function of the fourth power of the diameter of the aperture, which is attributed to the wavelength cutoff effect. Regular small apertures in circular and square shapes will suffer from extremely low power throughput that is insufficient for materials optical processing. Enhanced light transmission through small apertures is desired in order to be used as efficient transducers for radiation transfer.

Making a small aperture surrounded with periodic ring corrugations (bull's eye pattern) in noble metal films, the resonant transmission through the center aperture can be boosted by two orders of magnitude [6] relative to a bare aperture without any surrounding structures due to the resonant excitation of surface plasmon [7]. However, the high transmission efficiency of a hole smaller than 100 nm using this method has not been demonstrated yet. Another approach is to use a subwavelength aperture with a waveguide propagation mode supported in the aperture. In par-

ticular, ridge apertures in various shapes, i.e., C [8], I [9], or H [10,11], and bowtie [12,13] apertures, have been proposed to achieve nanoscale near-field radiation with enhanced optical transmission compared to regular small apertures. Ridge apertures have the specially designed geometry, which consists of a narrow gap connecting two side arms. The unique optical properties of ridge apertures benefit from the fundamental TE_{10} waveguide mode excited in the aperture channel, which has the transverse electric field confined within the nanometer-sized gap formed by the ridges and propagates through the aperture without experiencing much power loss [10].

Numerical simulations showed that C [8] and H [10] apertures made in a perfectly conducting plate provide enhanced power throughput of 2–3 orders of magnitude higher than that obtained by comparable conventional small square apertures. Detailed theories and numerical calculations of transmission enhancement and localization of radiated fields of ridged apertures can be found in Refs. [8–13]. The far-field radiation measurement of various apertures made in a gold film suggests C aperture shows an extraordinary transmission enhancement of about 10^6 over a conventional aperture of the same near-field resolution [14]. Furthermore, the confined optical near field of C aperture has also been experimentally demonstrated using near-field scanning optical microscope (NSOM) measurements [15]. This NSOM experiment [15] used an apertureless near-field probe, which scattered the radiated field from the C aperture.

In this paper, the near-field optical properties of an H -shaped ridge nanoaperture fabricated in an aluminum thin film are characterized using a specially designed aperture NSOM system. A cantilevered near-field probe with a nanoaperture at the end of the cantilever tip is used to directly map the near fields from the H aperture and conventional apertures of comparable sizes. The polarization dependence of near-field radiation from these apertures is investigated. The use of H apertures as highly efficient and reliable near-field transducers is demonstrated by imaging the optical near field from an array of H apertures. The experimental results are discussed and explained through finite difference time domain (FDTD) numerical computations together with the waveguide theory.

¹Contributed by the Heat Transfer Division of ASME for publication in the JOURNAL OF HEAT TRANSFER. Manuscript received January 23, 2006; final manuscript received June 16, 2006. Review conducted by M. Pinar Menguc.

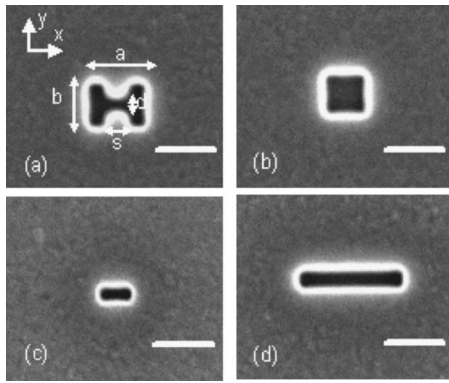


Fig. 1 SEM images of: (a) *H* aperture ($a=210$ nm, $b=170$ nm, $s=100$ nm, $d=60$ nm); (b) square aperture (160 nm by 160 nm); (c) small rectangular aperture (100 nm by 60 nm); and (d) large rectangular aperture (400 nm by 60 nm) fabricated in a 75 nm aluminum film on a quartz substrate. The scale bars are 200 nm.

2 Experimental Details

The *H* apertures and regular apertures of comparable sizes are fabricated in a thin aluminum film by focus ion beam (FIB) milling using a dual beam FIB machine (FEI Strata DB 235). The thickness of the aluminum film is 75 nm, which is deposited onto a quartz substrate by an *e*-beam evaporator. The scanning electron microscope (SEM) images of these fabricated apertures are shown in Fig. 1. The *H* aperture has an overall size of about 210 nm (a) \times 170 nm (b) with a small gap of 100 nm (s) \times 60 nm (d). The square and rectangular apertures are about 160 nm \times 160 nm, and 400 nm \times 60 nm in size, having roughly the same opening area as the *H* aperture. A 100 nm \times 60 nm regular aperture, which is supposed to provide the near-field optical spot of similar size as the *H* aperture, is also made for the purpose of comparison.

In order to retrieve the near-field information from these sub-wavelength apertures, a NSOM technique [16] has been employed. As shown in the schematic view (Fig. 2) of our aperture NSOM setup, the aluminum sample with fabricated apertures is illuminated by an argon-ion laser of about 2 mW power output at 458 nm wavelength from the substrate side. The spot size of the

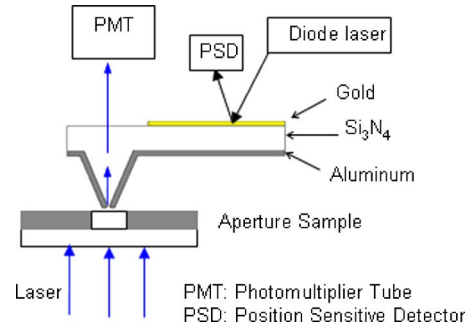


Fig. 2 Schematic view of the specially designed NSOM system using a cantilever aperture probe

laser beam on the sample is about 50 μ m. Because the near-field radiation from the subwavelength apertures in the sample is localized in the vicinity of the apertures, a near-field probe with a nanometer-sized aperture at the end is used and brought to the close proximity of the sample surface. It collects both nonpropagating and propagating components of the near-field radiation, and converts them to the propagating radiation which can be detected in the far field by a photomultiplier tube (PMT). The incident laser beam is adjusted to be polarized either in the y direction or the x direction as indicated in Fig. 1(a), and focused on the metal film. A NSOM image is obtained by raster scanning the apertures in the sample and recording the optical signal from the PMT by photon counting. During the sample scanning, the probe is in soft contact with the surface, which is achieved by maintaining a small and constant normal force (the tip-sample separation is typically in the 0–10 nm range) based on the cantilever feedback control by monitoring the deflected diode laser beam on the position sensitive detector (PSD).

The near-field aperture probe is the key element in this NSOM system. It determines the optical resolution that can be achieved. As shown in Fig. 3(a), the probe is in a pyramidal shape located near the end of a cantilever. It has a silicon nitride core coated with a thin aluminum film. An aperture of less than 100 nm in size at the apex of the probe is opened by FIB milling. To characterize the optical resolution of the NSOM measurements, the transmitted light from a pair of nanoholes in the same sample with known separation distances is collected by this probe. The obtained

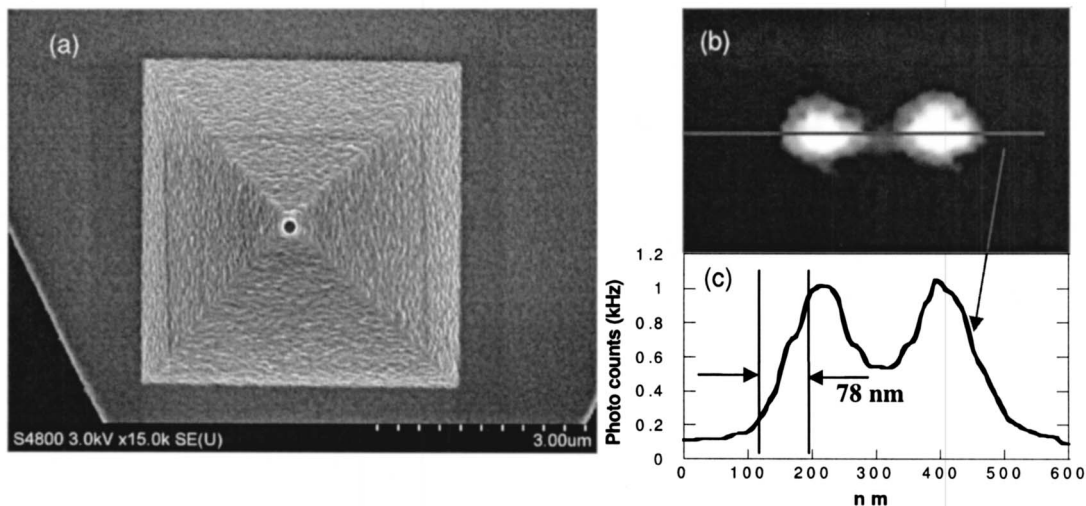


Fig. 3 (a) SEM image of cantilever aperture probe made by FIB milling; (b) NSOM image of a pair of nanoholes used to characterize the optical resolution the aperture probe; and (c) line scan on the NSOM image shows the 10–90% edge resolution of 78 nm

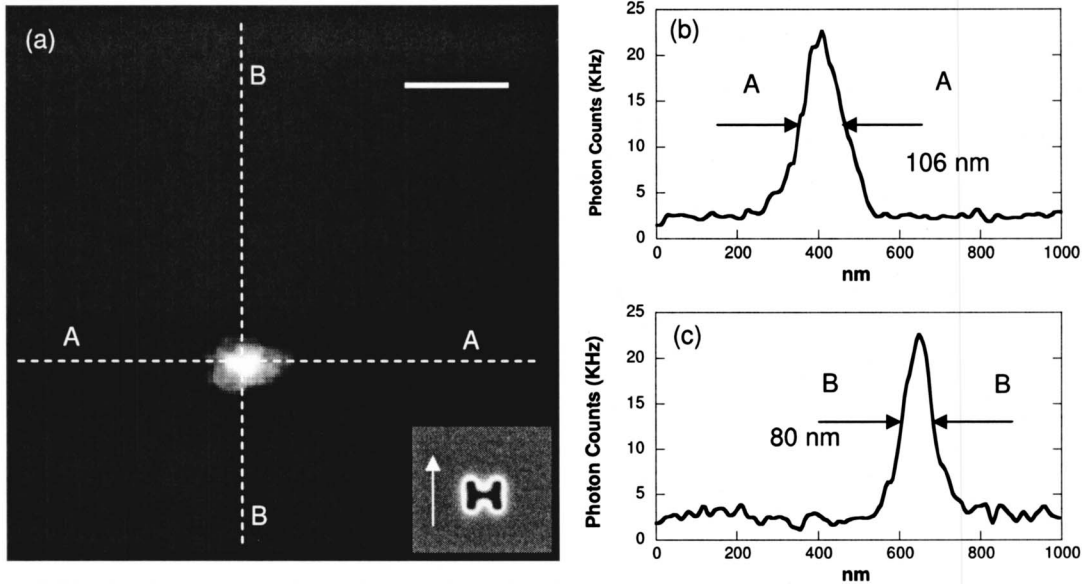


Fig. 4 (a) NSOM image of the H aperture ($210\text{ nm}\times 170\text{ nm}$ outline with a $100\text{ nm}\times 60\text{ nm}$ gap) and line scans in (b) A-A horizontal direction and (c) B-B vertical direction show the FWHM spot size is 106 nm by 80 nm . The illumination light is polarized along the y direction across the gap the H aperture as indicated in the inset of (a). The scale bar in (a) is 200 nm .

NSOM image is shown in Fig. 3(b). Figure 3(c) show the 10–90% edge resolution is about 78 nm by plotting the line scan profile of the NSOM signal as indicated in Fig. 3(b). This optical resolution is about $\lambda/6$ of the illumination light, and much less than the diffraction limit as expected.

3 Results and Discussion

3.1 NSOM Measurements. The near-field radiation from the H aperture and comparable conventional apertures is measured using the previously described NSOM system and the aperture probe of 78 nm optical resolution. Figure 4(a) shows the NSOM image obtained from the H aperture with the y polarized laser illumination. Since the overall tip size (the aperture opening surrounded by aluminum coating) of the probe is larger than the opening area of the H aperture, the probe could not get inside the aperture during the acquisition of the near-field signal. Therefore, the obtained NSOM image can be considered as a NSOM image performed at the constant height mode with a short distance ($0\text{--}10\text{ nm}$) away from the exit plane of the H aperture. The line scan analysis along the x and y directions is conducted as indicated on the two-dimensional NSOM image and plotted in Figs. 4(b) and 4(c), respectively. The full-width half-maximum (FWHM) of the near-field light spot is found to be 106 nm along the x direction (A-A shown in Fig. 4(b)), and 80 nm along the y direction (B-B shown in Fig. 4(c)). The actual spot size should be smaller due to the convolution effect of the aperture probe. Considering the symmetries of the H aperture geometry and near-field light spot, the near-field light through the H aperture is expected to be localized in the central gap between the ridges.

The near-field radiation from the conventional apertures of regular shapes is also acquired under the same illumination conditions. Figures 5(a) and 5(b) show the NSOM images for the square aperture and large rectangular aperture, respectively. The measured FWHM spot sizes are $136\text{ nm}\times 174\text{ nm}$ for the square aperture, and $212\text{ nm}\times 120\text{ nm}$ for the rectangular aperture. Both light spots are substantially larger than that achieved by the H aperture. The NSOM measurement of the small rectangular aperture, which has the same size as the gap of the H aperture and is

supposed to provide the near-field spot of similar size, was also attempted but failed to acquire sufficient light that can be detected by the measuring system. This indicates the expected low light transmission using the sub- 100 nm regular apertures. Since these apertures are separated from each other by a distance of more than $10\text{ }\mu\text{m}$, and thus the incident laser beam (diameter= $50\text{ }\mu\text{m}$) does not uniformly illuminate each aperture, the peak intensities of the NSOM spots from the apertures cannot be compared with each other. The relative transmission efficiencies through these apertures will be numerically investigated in the following section.

NSOM images of these apertures are also taken with the laser illumination polarized in the orthogonal direction or the x direction. It is found that both rectangular apertures do not produce enough light signals to form a NSOM image under this polarization. As shown in Fig. 6(b), a light spot of $167\text{ nm}\times 132\text{ nm}$ in FWHM size is achieved by the square aperture. The square aperture results in similar near-field spots in both polarizations as expected, and the elongation of the near-field spot is along the direction of laser polarization. The H aperture results in a $170\text{ nm}\times 188\text{ nm}$ light spot as shown in Fig. 6(a), which is significantly

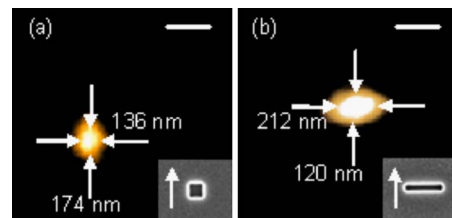


Fig. 5 NSOM images of: (a) the $160\text{ nm}\times 160\text{ nm}$ square aperture and (b) the $400\text{ nm}\times 60\text{ nm}$ rectangular aperture. The FWHM sizes of the near-field optical spots shown in the images are $174\text{ nm}\times 136\text{ nm}$ and $212\text{ nm}\times 120\text{ nm}$ for the square and rectangular apertures, respectively. The insets show the SEM pictures of the imaged apertures. The illumination light is polarized along the y direction as indicated in the insets. The scale bars are 200 nm .

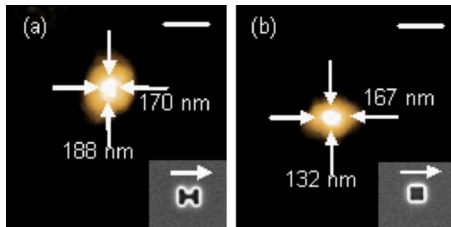


Fig. 6 NSOM images of: (a) the H aperture and (b) the $160\text{ nm}\times 160\text{ nm}$ square aperture. The FWHM sizes of the near-field optical spots shown in the images are $170\text{ nm}\times 188\text{ nm}$ and $167\text{ nm}\times 132\text{ nm}$ for the H and square apertures, respectively. The insets show the SEM pictures of the imaged apertures. The illumination light is polarized along the x direction as indicated in the insets. The scale bars are 200 nm .

larger than that is obtained under the y polarized illumination. This light spot almost covers the whole opening area of the H aperture, therefore no field concentration is provided by the H aperture when it is illuminated by light linearly polarized across the two open arms.

In comparison with the conventional apertures, the NSOM measurements clearly show that the H aperture is able to achieve the smallest light spot with considerable enhanced optical transmission under the proper polarization. The spot size is essentially determined by the gap size of the H aperture, as will also be seen from the FDTD results. It is therefore expected that further reduction of the gap size can produce a smaller light spot [11]. This makes H apertures as well as other ridge apertures attractive for use as an efficient near-field transducer for optical processing.

To examine the consistency and reliability of the NSOM results obtained by the H aperture, the optical near field from a 3×3 array of H apertures is measured. As shown in the SEM image (Fig. 7(a)) of the H aperture array fabricated in the same aluminum sample, the nine H apertures are almost identical and uniformly arranged in the array, and the variation in the dimensions of these apertures is less than 5 nm measured from the SEM image. Figure 7(b) shows the three-dimensional NSOM image collected under the laser illumination polarized in the direction across the gap of the H apertures. An array of clean light spots is obtained in the same pattern as the H aperture array. The average FWHM size of these nine light spots is $107\text{ nm}\times 84\text{ nm}$. The standard deviations of FWHM sizes are 4.7 nm in the x direction and 5.2 nm in y direction, corresponding to 4.4% and 6.1% size variation (relative standard deviation), respectively. In fact, the variation of near-field spot sizes is in the same order of the scanning resolution. The peak intensity value of these light spots has a 14% variation. These results indicate the consistency of near-field radiation from the H apertures as well as the reliability of the NSOM measurements.

3.2 FDTD Computations. In order to explain the experimental results, FDTD simulations are carried out to calculate the optical near field of each aperture, and also to illustrate how the light propagates through each aperture. The detailed description of the FDTD numerical method can be found in the Refs. [17,18]. In the following FDTD computations, the dimensions of each aperture are chosen based on the measurement of the SEM images. Both the optical property of the aluminum at 458 nm [19] and the change of laser polarization are considered.

Figure 8 shows the FDTD results for the H aperture, square aperture, and large rectangular aperture under the y polarized illuminating light at 458 nm wavelength. The left column shows the near-field intensity distribution on the xy plane at 10 nm below the three apertures. Two hot spots can be seen for all three apertures, which were not observed in the NSOM measurements. The difference could arise from two possibilities. First, the aper-

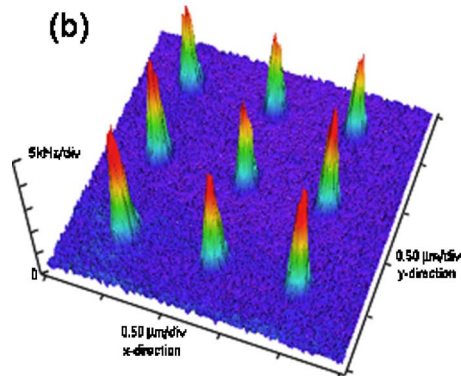
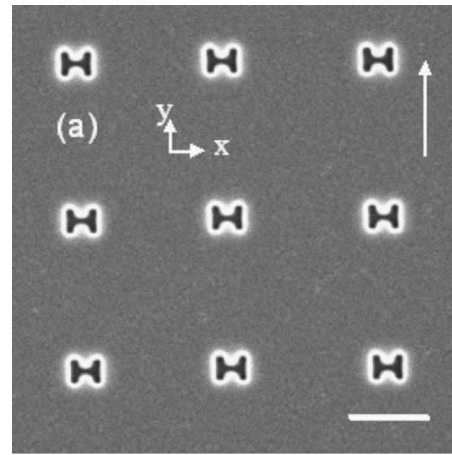


Fig. 7 (a) SEM image of an array of H apertures fabricated in an aluminum film and (b) three-dimensional NSOM image of the array. The illumination light is polarized along the y direction across the gap of the H apertures as indicated by the arrow in the inset of (a). The scale bar in (a) is 500 nm .

tures used in the calculations have sharp edges while the fabricated ones have round edges. In fact, the sharp edges induce the z component of the electric field in the FDTD calculations along the polarization direction due to the scattering effect [13]. Second, the optical resolution of the aperture probe is not likely enough to resolve the two hot spots. The NSOM spot is the convolution of the scanning probe transfer function with the actual near-field light spot transmitted through the measured aperture. It is only when the probe is a point source (representing a delta function) that the measured NSOM spot is exactly the same as the actual near-field spot assuming the probe does not disturb the radiating field. On the other hand, the numerical results clearly show that the H aperture confines the near-field radiation underneath the gap region and results in the smallest light spot in both lateral directions compared to the other two apertures. This is consistent with the NSOM measurements. The right column of Fig. 8 shows how light propagates through the three apertures. Both the H aperture and rectangular aperture have a propagating waveguide mode in the aperture channels (Figs. 8(b) and 8(f)), which provides the efficient transmission through these apertures. The existence of waveguide mode in these two apertures is because the incident wavelength is shorter than the cutoff wavelengths of the apertures [10]. By either elongating the small rectangular aperture (to become the large rectangular aperture) or adding two side arms to it (to become the H aperture), the cutoff wavelength of the aperture will be significantly increased. An evanescent mode with the field intensity decaying exponentially is found inside the square aperture as shown in Fig. 8(d). However, because the illumination wavelength of 458 nm is close to the cutoff wavelength of the

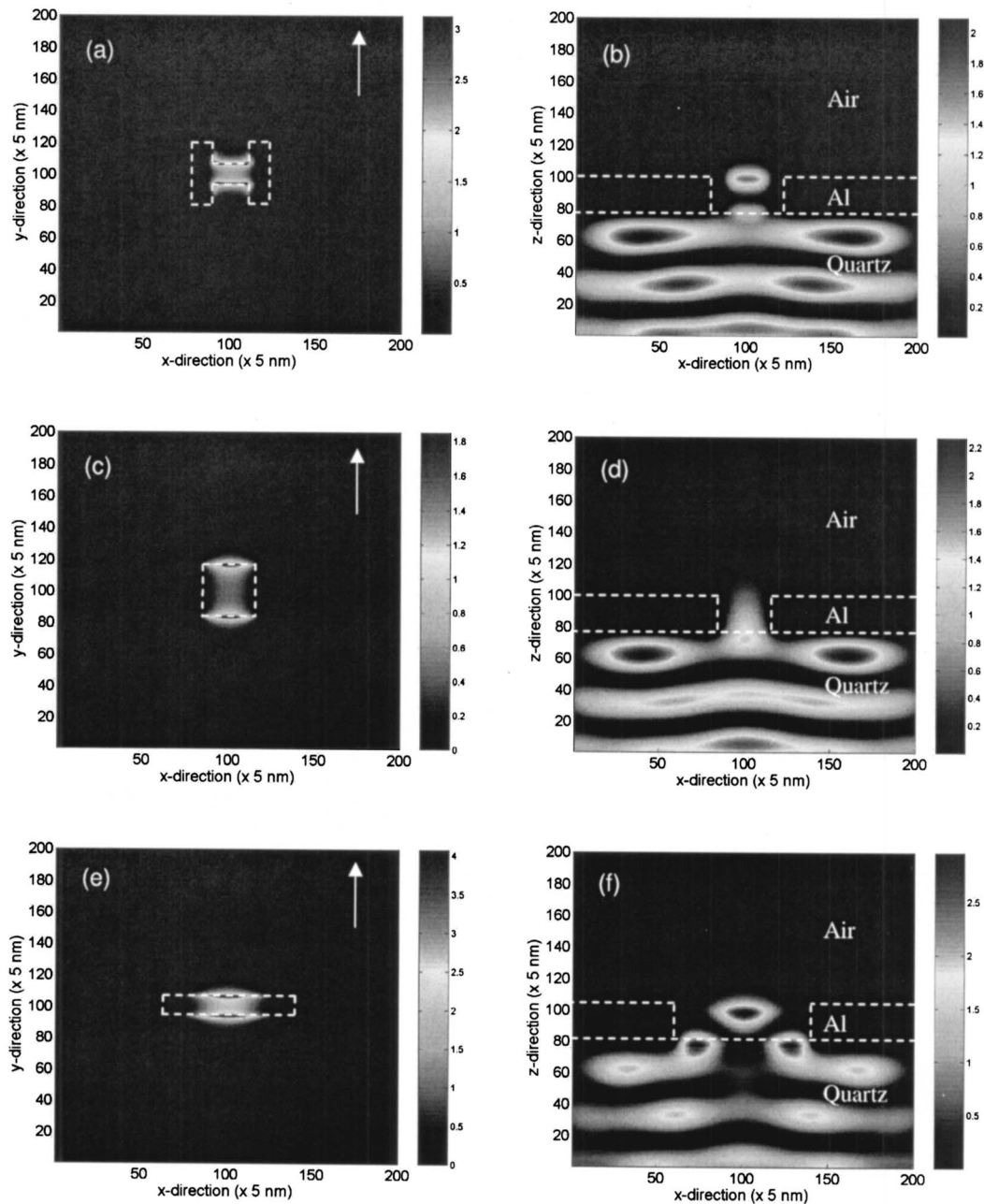


Fig. 8 Left column: the computed near-field intensity distribution (normalized by incident intensity) on the xy plane at 10 nm below (a) the H aperture; (c) the square aperture; and (e) the rectangular aperture in a 75-nm-thick aluminum film on a quartz substrate. Right column: light propagation on the xz plane through the middle of (b) the H aperture; (d) the square aperture; and (f) the rectangular aperture. The y polarized plane wave at 458 nm wavelength is incident from the quartz side. The arrows indicate the polarization direction of the incident light.

square aperture [20], a small attenuation of the transmitted field results. There are still enough photons tunneling through the sub-wavelength square aperture and resulting in signals that can be detected by the PMT. The integrated intensities over a $400 \text{ nm} \times 170 \text{ nm}$ area at 10 nm below the H ; square, large rectangular, and small rectangular apertures are 938, 610, 1761, and 45, respectively (the incident integrated intensity over the same area is 2720). Therefore, the H aperture is able to provide the smallest optical spot with the light transmission on the same order of those through the regular apertures of the same opening area, but 20 times that through the smallest rectangular aperture. According to the standard aperture theory [5], the transmission efficiency

through the small rectangular aperture will be greatly decreased by further reducing its size in order to achieve a smaller optical spot. The H aperture, on the other hand, can maintain the transmission efficiency (on the order of unity) when the gap size is further reduced due to the existence of the propagating waveguide mode.

The FDTD results for the x -polarized illumination are shown in Fig. 9. Due to the symmetry of its geometry, the same result as for the y polarization is expected for the square aperture, therefore is not computed. It is clearly seen a greatly attenuated evanescent mode in the rectangular aperture in Fig. 9(d). This can be again explained by the waveguide cutoff calculation [20]: the illumina-

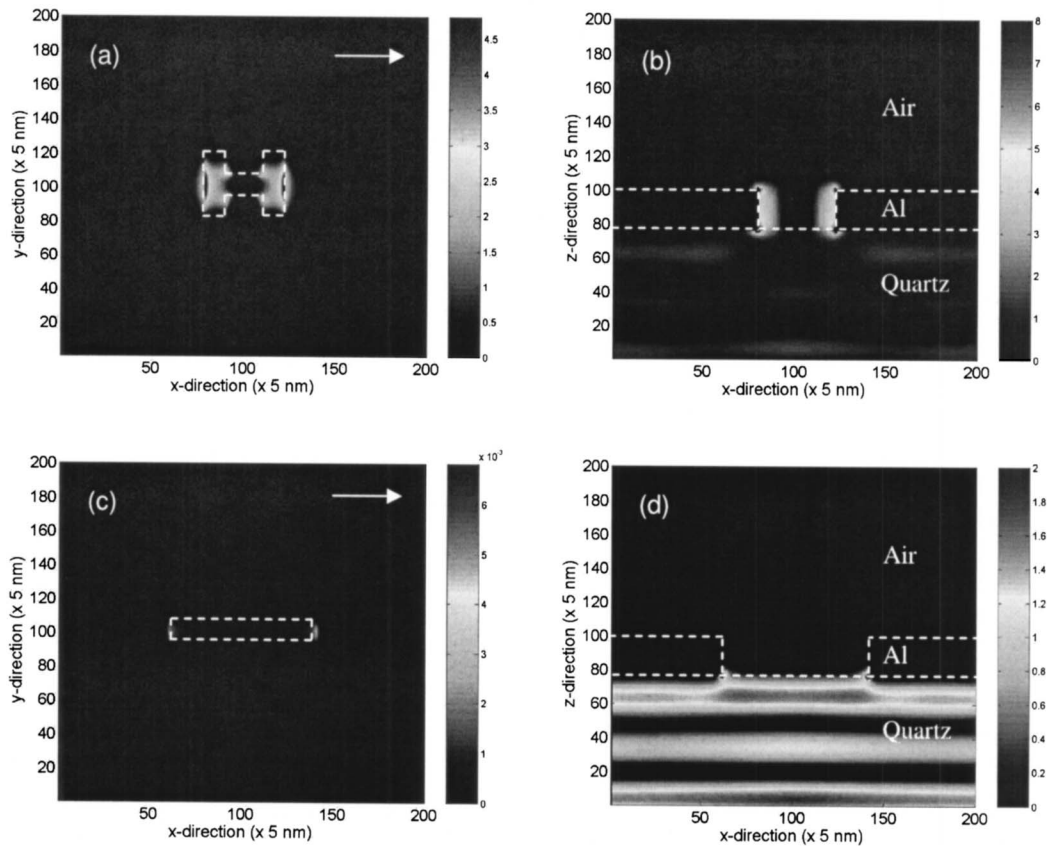


Fig. 9 Left column: the computed near-field intensity distribution (normalized by incident intensity) on the xy plane at 10 nm below (a); the H aperture, and (c) the square aperture in a 75-nm-thick aluminum film on a quartz substrate. Right column: light propagation on the xz plane through the middle of (b) the H aperture, and (d) the rectangular aperture. The x polarized plane wave at 458 nm wavelength is incident from the quartz side. The arrows indicate the polarization direction of the incident light.

tion wavelength is much larger than the cutoff wavelength of the rectangular aperture under the x -polarized illumination resulting in a large attenuation coefficient. In this case, the rectangular aperture looks like the other part of the aluminum film so that most of the incident photons are reflected back. The field intensity below the aperture is three orders less than that of the incident one as shown in Fig. 9(c) because only a few photons can tunnel through the short aperture channel. On the other hand, the H aperture is still able to provide a strong radiating field at the exit side whose intensity is in the same order of the incidence as shown in Fig. 9(a). This is because the two open arms of the H aperture act as propagating waveguides under this polarization. The surface waves are found on the side walls in the aperture channel, therefore allowing a large amount of light through the aperture as shown in Fig. 9(b). It is also found that the near-field spot of the H aperture under x polarization illumination is considerably larger than that in the y polarization illumination. These FDTD results at x polarization are all consistent with the NSOM observations.

4 Conclusions

In summary, the near-field radiation from the H -shaped apertures and conventional apertures of comparable sizes fabricated in a 75-nm-thick aluminum film is characterized using a specially designed aperture NSOM system with the optical resolution around 80 nm. FDTD numerical computations are used to explain the NSOM observations. It is found that the H aperture is able to provide a $106 \text{ nm} \times 80 \text{ nm}$ optical spot when the incident light at 458 nm is polarized along the direction across the gap. A 4–6% FWHM size variation and a 14% intensity variation of near-field

spots from a 3×3 array of H apertures are obtained, showing the consistency and reliability of the near-field radiation from the fabricated H apertures. The H aperture results in a larger spot under the x -polarized illumination light. Compared to the square aperture and the rectangular of the same opening area, the H aperture provides a substantially smaller near-field light spot without suffering the low light transmission, which allows many promising applications in near-field nanoscale optical engineering.

Acknowledgment

The financial support to this work by the Office of Naval Research and the National Science Foundation is gratefully acknowledged. Fabrications of aperture sample and aperture probe by FIB milling were carried out in the Center for Microanalysis of Materials, University of Illinois, which is partially supported by the U.S. Department of Energy.

Nomenclature

- a = length of the H aperture
- b = width of the H aperture
- d = gap width of the H aperture
- s = gap length of the H aperture
- λ = wavelength of light/laser
- E = electric field

References

- [1] Mansfield, S. M., Studenmund, W. R., Kino, G. S., and Osato, K., 1993, "High Numerical-Aperture Lens System for Optical Data Storage," *Opt. Lett.*, **18**(4),

- pp. 305–307.
- [2] Betzig, E., Trautman, J. K., Wolfe, R., Gyorgy, E. M., Finn, P. L., Kryder, M. H., and Chang, C. H., 1992, “Near-Field Magneto-Optics and High Density Data Storage,” *Appl. Phys. Lett.*, **61**, pp. 142–144.
 - [3] Peng, C., Mihalcea, C., Buchel, D., Challener, W. A., and Gage, E. C., 2005, “Near-Field Optical Recoding Using a Planar Solid Immersion Mirror,” *Appl. Phys. Lett.*, **87**, pp. 151105-1–151105-3.
 - [4] Partovi, A., Peale, D., Wuttig, M., Murray, C. A., Zydzik, G., Hopkins, L., Baldwin, K., Hobson, W. S., Wynn, J., Lopata, J., Dhar, L., Chichester, R., and Yeh, J. H.-J., 1999, “High-Power Laser Light Source for Near-Field Optics and its Application to High-Density Optical Data Storage,” *Appl. Phys. Lett.*, **75**, pp. 1515–1517.
 - [5] Bethe, H., 1944, “Theory of Diffraction by Small Holes,” *Phys. Rev.*, **66**, pp. 163–182.
 - [6] Thio, T., Pellerin, K. M., Linke, R. A., Lezec, H. J., and Ebbesen, T. W., 2001, “Enhanced Light Transmission Through a Single Subwavelength Aperture,” *Opt. Lett.*, **26**(24), pp. 1972–1974.
 - [7] Raether, H., 1988, *Surface Plasmons on Smooth and Rough Surfaces and on Gratings*, Springer, Berlin, Germany.
 - [8] Shi, X., and Hesselink, L., 2002, “Mechanisms for Enhancing Power Throughput from Planar Nano-Apertures for Near-Field Optical Data Storage,” *Jpn. J. Appl. Phys., Part 1*, **41**(3B), pp. 1632–1635.
 - [9] Tanaka, K., and Tanaka, M., 2003, “Simulation of an Aperture in the Thick Metallic Screen that Gives High Intensity and Small Spot Size Using Surface Plasmon Polariton,” *J. Microsc.*, **210**, pp. 294–300.
 - [10] Jin, E. X., and Xu, X., 2004, “FDTD Studies on Optical Transmission Through Planar Nano-Apertures in a Metal Film,” *Jpn. J. Appl. Phys., Part 1*, **43**(1), pp. 407–417.
 - [11] Jin, E. X., and Xu, X., 2005, “Radiation Transfer Through Nanoscale Apertures,” *J. Quant. Spectrosc. Radiat. Transf.*, **93**, pp. 163–173.
 - [12] Sendur, K., and Challener, W., 2003, “Near-Field Radiation of Bow-Tie Antennas and Apertures at Optical Frequencies,” *J. Microsc.*, **210**, pp. 279–283.
 - [13] Jin, E. X., and Xu, X., 2005, “Obtaining Super Resolution Light Spot Using Surface Plasmon Assisted Sharp Ridge Nanoaperture,” *Appl. Phys. Lett.*, **86**, pp. 111106-1–111106-3.
 - [14] Matteo, J. A., Fromm, D. P., Yuen, Y., Schuck, P. J., Moerner, W. E., and Hesselink, L., 2004, “Spectral Analysis of Strongly Enhanced Visible Light Transmission Through Single C-Shaped Nanoapertures,” *Appl. Phys. Lett.*, **85**, pp. 648–650.
 - [15] Chen, F., Itagi, A., Bain, J. A., Stancil, D. D., Schlesinger, T. E., Stebounova, L., Walker, G. C., and Akhremitchev, B. B., 2003, “Imaging of Optical Field Confinement in Ridge Waveguides Fabricated on Very-Small-Aperture Laser,” *Appl. Phys. Lett.*, **83**, pp. 3245–3247.
 - [16] Courjon, D., 2003, *Near-Field Microscopy and Near-Field Optics*, Imperial College Press, London, UK.
 - [17] Kunz, K., and Luebbers, R., 1996, *The Finite Difference Time Domain Method for Electromagnetics*, CRC, Boca Raton, FL.
 - [18] Taflov, A., 1995, *Computational Electrodynamics: The Finite-Difference Time-Domain Method*, Artech House, Boston, MA.
 - [19] Lide, D. R., 1996, *CRC Handbook of Chemistry and Physics*, CRC, Boca Raton, FL.
 - [20] Gordon, R., and Brolo, A. G., 2005, “Increased Cut-off Wavelength for a Subwavelength Hole in a Real Metal,” *Opt. Express*, **13**(6), pp. 1933–1938.